

## Ballistics of self-jumping microdroplets

P. Lecointre, C. Black

To be published in "JOVE-JOURNAL OF VISUALIZED EXPERIMENTS"

September 2018

Center for Functional Nanomaterials  
**Brookhaven National Laboratory**

**U.S. Department of Energy**  
USDOE Office of Science (SC), Basic Energy Sciences (BES) (SC-22)

Notice: This manuscript has been authored by employees of Brookhaven Science Associates, LLC under Contract No. DE-SC0012704 with the U.S. Department of Energy. The publisher by accepting the manuscript for publication acknowledges that the United States Government retains a non-exclusive, paid-up, irrevocable, world-wide license to publish or reproduce the published form of this manuscript, or allow others to do so, for United States Government purposes.

## **DISCLAIMER**

This report was prepared as an account of work sponsored by an agency of the United States Government. Neither the United States Government nor any agency thereof, nor any of their employees, nor any of their contractors, subcontractors, or their employees, makes any warranty, express or implied, or assumes any legal liability or responsibility for the accuracy, completeness, or any third party's use or the results of such use of any information, apparatus, product, or process disclosed, or represents that its use would not infringe privately owned rights. Reference herein to any specific commercial product, process, or service by trade name, trademark, manufacturer, or otherwise, does not necessarily constitute or imply its endorsement, recommendation, or favoring by the United States Government or any agency thereof or its contractors or subcontractors. The views and opinions of authors expressed herein do not necessarily state or reflect those of the United States Government or any agency thereof.

# Ballistics of self-jumping microdroplets

Pierre Lecointre<sup>1,2</sup>, Timothée Mouterde<sup>1,2</sup>, Antonio Checco<sup>3</sup>, Charles T. Black<sup>4</sup>,  
Atikur Rahman<sup>5</sup>, Christophe Clanet<sup>1,2</sup>, and David Quéré<sup>\*1,2</sup>

<sup>1</sup>Physique et Mécanique des Milieux Hétérogènes, UMR 7636 du CNRS, ESPCI, 75005 Paris, France.

<sup>2</sup>Laboratoire d'Hydrodynamique de l'X, UMR 7646 du CNRS, École polytechnique, 91128 Palaiseau, France.

<sup>3</sup>Mechanical Engineering Department, Stony Brook University, Stony Brook NY 11794, USA.

<sup>4</sup>Center for Functional Nanomaterials, Brookhaven National Laboratory, Upton NY 11973, USA.

<sup>5</sup>Department of Physics, Indian Institute of Science Education and Research (IISER)-Pune, Maharashtra 411008,  
India.

Water-repellent materials ideally operate at very different liquid scales - from centimeter-size for bugs living on ponds through millimeter-size for anti-rain functions to micrometer-size for anti-fogging solids. In the latter situation, it was recently evidenced that microdrops condensing on a highly non-adhesive substrate can take advantage from coalescence to jump off the material, even if the dynamical characteristics of the jump were not established at such microscales. We demonstrate in this paper that the jumping speed of drops is non-monotonic with the drop size, showing a maximum around  $5 \mu\text{m}$  (a size commonly observed in dew) - below and above which viscous and inertial effects, respectively, impede the takeoff. We quantitatively describe this optimum in anti-fogging. We also studied the ballistics of the jumping microdrops, from the height they reached to their behavior at landing - a situation where re-takeoff is surprisingly found to be nearly unachievable despite the extreme non-wettability of the material.

---

\*Corresponding author

# Introduction

Water-repellent materials provide a wide variety of functions, which makes them ubiquitous in the natural world. Such materials allow creatures to live at the surface of water [1–3] and they also repel water in dynamic conditions (rain) by efficiently reflecting impacting millimetric drops [4–6]; these surfaces are also superaerophilic when immersed in water [7], a property that provides oxygen resources for underwater animals, thermal insulation [8–10], anti-biofouling and slip properties [11–14]. Among these properties, one of the most challenging ones might be the ability to repel water at a micrometric scale, that is, at the scale of the textures responsible for superhydrophobicity. However, it was recently shown that nanotextured surfaces may self-remove condensing water [15, 16]: growing droplets coalesce and the excess of surface energy can lead to the departure of the resulting drop. Considering that surface energy is converted into kinetic energy, the jumping velocity  $U$  of the merged drop scales as  $\sqrt{\gamma/\rho r}$ , denoting  $\gamma$  as the liquid surface tension,  $\rho$  as its density and  $r$  as the radius of the coalescing droplets [15, 17, 18]. It was first reported that only droplets with radius greater than  $10\ \mu\text{m}$  can depart from the substrate [15]. Below this critical radius ( $\approx 10\ \mu\text{m}$ ), internal viscous dissipation during coalescence was proposed to impede the motion [17, 19].

However, recent experimental and numerical studies have proved that jumping can occur at a much smaller scale, for  $r \approx 5\ \mu\text{m}$  [20, 21],  $r \approx 1\ \mu\text{m}$  [22, 23] and even  $r \leq 500\ \text{nm}$  [18, 24–26]. Both this threshold and the jumping velocity are material-dependent [17, 19, 23, 26], and modelling them requires to consider both viscous and adhesive effects at such microscales. Our first aim in this paper is to shed light on this issue, based on experiments performed on special textures on which coalescing microdrops systematically take off [22]. We then describe the flight of such expelled drops from merging and departure to their return to the material. In our investigations, we measure the maximum height reached by the jumping water, which in natural cases must be large enough to leave the air boundary layer and to allow the drop to go with the wind - a condition for achieving a genuine antifogging material [16, 27–30].

We first consider water condensation on a silicon surface covered with nanocones inspired by the textures found on cicada wings [16] (Figure 1a). These surfaces are fabricated by combining block-copolymer self-assembly with anisotropic plasma etching [31]. The resulting cones have a base diameter of  $52\ \text{nm}$  and a height of  $115\ \text{nm}$ , and they are disposed in a dense hexagonal array. Chemical vapour deposition of 1H,1H,2H,2H-perfluorodecyltrichlorosilane makes the surface hydrophobic. This treatment on flat silicon gives an advancing water contact angle  $\theta_0 = 120 \pm 2^\circ$ , a value that jumps to  $\theta_a = 167 \pm 2^\circ$  on the nanocones. The corresponding receding angle is  $\theta_r = 157 \pm 2^\circ$ , which entails a modest hysteresis  $\Delta\theta = \theta_a - \theta_r = 10 \pm 4^\circ$ . Condensation of water

from the atmosphere is triggered by affixing the substrate on a Peltier module, and setting the temperature at  $T_s = 3 \pm 1^\circ\text{C}$ , a value below the dew point in the laboratory conditions (temperature  $T = 25 \pm 1^\circ\text{C}$  and relative humidity  $RH = 39 \pm 1\%$ , supersaturation is  $S = 1.63 \pm 0.26$ ).

## Symmetrical merging

Our experiment, sketched in Figure 1b, consists of filming the coalescence of pairs of neighbouring condensed droplets, simultaneously from above and from aside. Images are captured using synchronized high-speed video-cameras (Photron Fastcam Mini UX100) at a respective rate of 1 kHz and 40 kHz for top and side views and connected to a microscope (Infinitube In-line and Nikon ELWD 20x). The top view allows us to measure the radii of merging droplets, respectively denoted as  $r$  and  $r'$  ( $r' < r$ ), and to check that only two-droplet coalescences are considered. We first focus on symmetric situations for which the radii ratio  $\varepsilon = r'/r$  is larger than 0.95. The takeoff velocity  $U$  is deduced from side views. The drop's position is computed for each frame and  $U$  is deduced from measurements performed on the first 5 snapshots, just after takeoff. A layer of microdroplets sometimes hides the beginning of the jump, which generates uncertainty on the takeoff time and ultimately a 5% uncertainty on  $U$ .

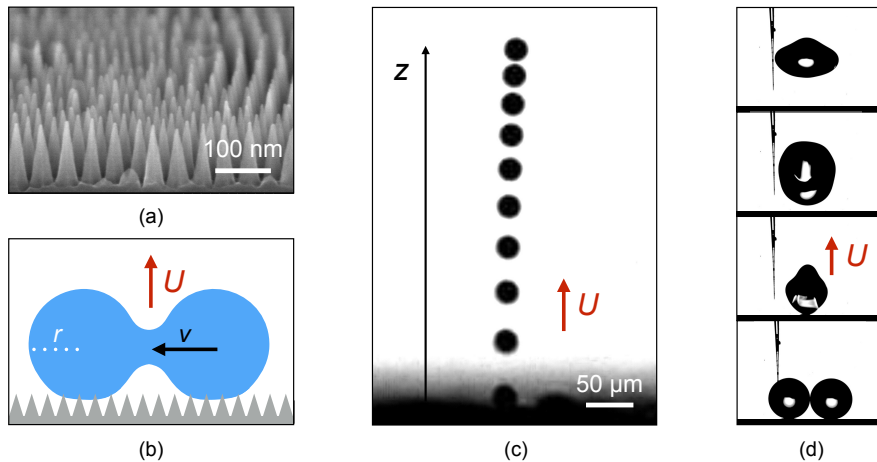


**Figure 1.** (a) Scanning electron micrograph of the nanocones used in this study. The scale indicates 100 nm. (b) Sketch of two non-wetting droplets with radius  $r$  merging at a velocity  $v$  on hydrophobic nanocones; the jumping velocity of the resulting drop is denoted as  $U$ . (c) Side-view chronophotography of a jumping drop with radius  $R = 11.3 \pm 0.1 \mu\text{m}$  resulting from the coalescence of a pair of droplets with  $r = 8.9 \pm 0.1 \mu\text{m}$ . Images are separated by 0.125 ms. The drop takes off with a vertical jumping velocity  $U = 55 \pm 5 \text{ cm/s}$ . (d) High-speed photography of a symmetric coalescence of two drops with  $r = 580 \pm 5 \mu\text{m}$ . Images are separated by 3.7 ms, except the last one which is at 15.5 ms, when the drop reaches its maximum height. The first snapshot (at the bottom) shows the beginning of the coalescence while the second one corresponds to takeoff; the measured jumping velocity is  $U = 7 \pm 1 \text{ cm/s}$ .

A typical experiment is shown in the chronophotography of Figure 1c. We observe the takeoff of a water drop with radius  $R = 11.3 \pm 0.1 \mu\text{m}$  resulting from the symmetric coalescence of a pair of droplets with  $r = 8.9 \pm 0.1 \mu\text{m}$ . We deduce from successive snapshots the jumping velocity  $U = 55 \pm 5 \text{ cm/s}$ , and the trajectory  $z(t)$  after departure. Water first strongly accelerates (with a

typical acceleration of 1000 g) and then decelerates over a distance of only 400  $\mu\text{m}$ , resulting from the efficient resistance of air at the scale of microdroplets. Small airflows cause the trajectory to deviate slightly from the vertical, another consequence of the small drop size.

The high antifogging ability of these substrates allows us to observe the departure of droplets with radii  $r$  spanning from 1.3  $\mu\text{m}$  to 24  $\mu\text{m}$  [22]. We complemented this interval by also measuring the coalescence of needle-dispensed drops with radii ranging from 150  $\mu\text{m}$  to 1100  $\mu\text{m}$ . For this second series of experiments, a first droplet is dispensed from a superhydrophobic glass micro-needle and a second one is made the same way until merging occurs, which is recorded from the side at a rate of 4 kHz. The resulting jumping velocity  $U$  is obtained as previously, but with larger time steps to filter the interface oscillations. Figure 1d shows the takeoff after merging of two drops with radius  $r = 580 \pm 5 \mu\text{m}$ . The departure velocity is  $U = 7 \pm 1 \text{ cm/s}$ , much smaller than observed for smaller drops (Figure 1c). In addition, we notice strong persistent droplet deformations after coalescence, another consequence of the much larger scale.

The evolution of the jumping velocity  $U$  after symmetric coalescence between two drops with radius  $r$  is reported in Figure 2a. We distinguish two families of data that respectively correspond to condensation ( $r \leq 24 \mu\text{m}$ ) and deposition ( $r \geq 150 \mu\text{m}$ ). For  $r > 5 \mu\text{m}$ ,  $U$  decreases as  $r$  increases and the data are well-described by the dotted line with slope  $-0.5$  on the log-log plot. "Large" drops depart with the inertio-capillary velocity  $U \sim \sqrt{\gamma/\rho r}$ , as reported by several authors [15, 18, 24], a law extended here down to 5  $\mu\text{m}$ . However, drops smaller than 5  $\mu\text{m}$  take off slower than predicted by this scaling and  $U$  tends to 0 as  $r$  approaches 1  $\mu\text{m}$ , in agreement with the cut-off radius measured on the same substrate in [22].

The inertio-capillary velocity is generally derived by considering that surface energy is transferred into kinetic energy, an argument that yields  $U = (3 [2 - 2^{2/3}])^{1/2} U^* \approx 1.11U^*$ , denoting  $U^* = \sqrt{\gamma/\rho r}$ . While we observe  $U$  scaling as  $r^{-1/2}$ , this relation overestimates the observed speed by a factor of order 5, as seen in Figure 2a where the law  $U = 1.11U^*$  is drawn as a black solid line. Mouterde *et al.* [32] showed that this discrepancy can be removed by expressing the balance of forces during merging. Each droplet retracts at a velocity  $v \approx r/\tau$ , where  $\tau \approx 2\sqrt{\rho r^3/\gamma}$  is the inertio-capillary duration of coalescence. Transfer of momentum can be written  $2mU = mv$  (denoting  $m = (4\pi/3)\rho r^3$ , the mass of each merging droplet), which yields  $U = U^*/4$ . This velocity has the same scaling form as  $U^*$ , but its numerical coefficient is 1/4 instead of 1.11. The best fit coefficient for the data in Figure 2a is 0.22, 10 % smaller than 1/4. A possible origin for this slight discrepancy arises from the typical energy  $E_a = \pi r^2 \gamma \sin^2 \theta_r (1 + \cos \theta_r)$  needed to detach each droplet from the substrate. Each corresponding momentum can be written  $P_a \approx E_a \tau / r$ , which modifies the takeoff velocity in  $U = (U^*/4) [1 - 6 \sin^2 \theta_r (1 + \cos \theta_r)]$ . A numerical coeffi-

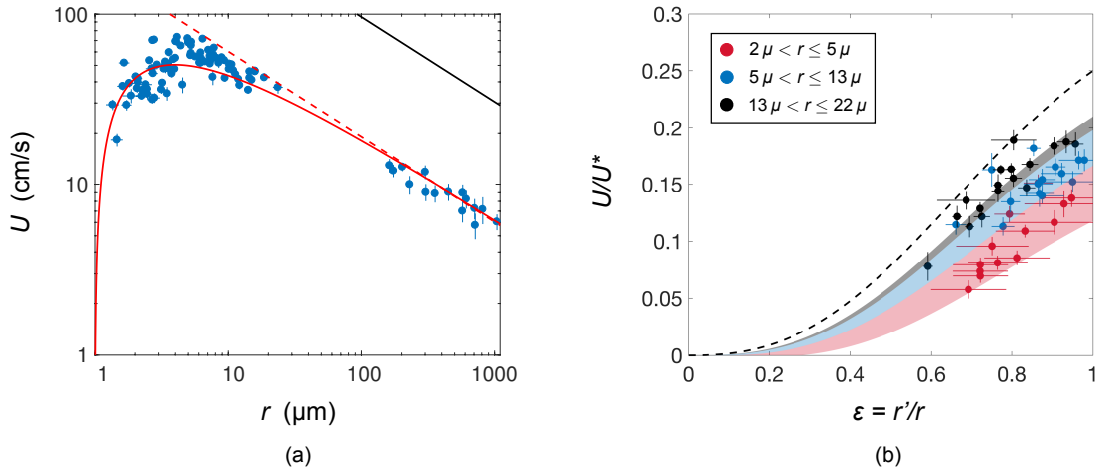


**Figure 2. Jumping velocity resulting from the coalescence of two droplets.** (a) Velocity  $U$  for symmetric coalescence ( $\varepsilon > 0.95$ ) as a function of the radius  $r$  of the two merging drops. Black line shows the speed resulting from energy conservation ( $U = 1.11U^*$ ) and red dashed line corresponds to  $U = 0.22U^*$ , denoting  $U^* = \sqrt{\gamma/\rho r}$ . The red line shows the velocity  $U = (U^*/4) [\alpha - 4.9 Oh]$  where  $\alpha = 1 - 6 \sin^2 \theta_r (1 + \cos \theta_r)$  and  $Oh = \eta/\sqrt{\rho \gamma r}$  is the Ohnesorge number with  $\eta$  the water viscosity. The coefficient of  $Oh$  is 4.9, a value close to the one predicted by momentum balance and shown in Eq. 1. (b) Jumping velocity of droplets after an asymmetric coalescence;  $U$  is normalized by  $U^* = \sqrt{\gamma/\rho r}$  and plotted as a function of the degree of symmetry  $\varepsilon = r'/r$ . The three sets of data correspond to three ranges for the large radius  $r$ :  $2\ \mu\text{m} < r \leq 5\ \mu\text{m}$  (red),  $5\ \mu\text{m} < r \leq 13\ \mu\text{m}$  (blue) and  $13\ \mu\text{m} < r \leq 22\ \mu\text{m}$  (black). The dashed line shows  $U/U^* = \varepsilon^{5/2}/2(1 + \varepsilon^3)$  a function given by momentum conservation and neglecting adhesion and viscous dissipation [32], which provides an asymptotical behaviour for the data. Red, blue and black areas show Eq. 2 drawn with the corresponding colours for each range of radii.

cient of 0.22 corresponds to a receding angle of  $154^\circ$ , a value comparable to the measured angle  $\theta_r = 157 \pm 2^\circ$ . This small correction in coefficient suggests that water adhesion remains marginal in our system.

The dotted line in Figure 2a fairly matches the data obtained at "large" radius ( $r > 5\ \mu\text{m}$ ), which suggests that water remains in the Cassie state despite condensation [22, 33]. Water nuclei growing within conical textures are brought to the top of the surface by Laplace pressure. A few nanodroplets might remain pinned within the forest of cones, which could explain that the dotted line in Figure 2a slightly overestimates some data in this region. However, adhesion remains marginal at both large and small scales, which explains that about 99 % of merging microdroplets take off from nanocones arrays [22].

However, the takeoff velocity  $U$  of droplets smaller than  $5\ \mu\text{m}$  deviates strongly from the relationship described by the dotted line in Figure 2a. In the absence of significant adhesion, we interpret this decrease in mobility by considering the effect of viscosity. The flow during coalescence generates a dissipative force per droplet  $F_v \approx \eta \Delta v \Omega$ , where  $\eta$  is the viscosity of water and  $\Omega$  the droplet volume. Since  $\Delta v$  scales as  $v/r^2$ , we deduce  $F_v \approx (\pi\eta/3)(\gamma r/\rho)^{1/2}$ , an expression that depends on both viscosity and radius. The resulting loss of momentum  $P_v \approx F_v \tau$  is found to be  $(4\pi/3)\eta r^2$ . For  $r \approx 5\ \mu\text{m}$  and  $U \approx 50\ \text{cm/s}$ , the ratio  $P_v/mU$  is of order unity and it decreases

as  $1/\sqrt{r}$ , which suggests that viscous dissipation is indeed the main cause of loss at microscales. This result qualitatively agrees with numerical simulations that showed that water should be fully immobilized at a scale smaller than 300 nm [18, 24].

Taking losses into account, the momentum balance becomes:  $2mU = mv - 2P_v - 2P_a$ , where the factor 2 refers to the number of merging droplets. These considerations yield a modified expression for the jumping velocity  $U$ :

$$U \approx U^* \left[ \frac{\alpha}{4} - Oh \right] \quad (1)$$

where we have introduced the Ohnesorge number  $Oh = \eta/(\rho\gamma r)^{1/2}$  and where  $\alpha = 1 - 6 \sin^2 \theta_r (1 + \cos \theta_r)$  is a numerical coefficient close to unity at large  $\theta_r$ . It is interesting to note that an energy conservation argument leads to a normalized velocity  $U/U^*$  scaling as  $\sqrt{1 - Oh}$  [17, 19, 34], a power law much different from the one obtained with momentum transfer (Eq. 1). Eq. 1 is drawn in Figure 2a with a red solid line with  $\alpha \approx 0.93$  (corresponding to the measured value  $\theta_r = 157^\circ$ ) and using 4.9 instead of 4 for the coefficient of viscosity for the best fit to the data. We used  $\eta = 1.62$  mPa.s,  $\rho = 1000$  kg/m<sup>3</sup> and  $\gamma = 75.3$  mN/m, all quantities considered for water at 3°C. Eq. 1 nicely captures the decrease of the departing velocity for  $r \lesssim 5 \mu\text{m}$ , *i.e.* for  $Oh \gtrsim 0.1$ , showing how viscosity affects the inertio-capillary scenario. In addition, this expression predicts a critical jumping radius of 1  $\mu\text{m}$  and a maximum jumping velocity  $U$  for  $r \approx 4 \mu\text{m}$ , in good agreement with the experiments. For  $r \geq 150 \mu\text{m}$ , the predicted velocity approaches  $U = 0.22U^*$ , the asymptotic behaviour drawn with a dotted line.

## Asymmetrical merging

Condensing droplets are often asymmetric when they merge, due to the randomness of the condensation process. In Figure 2b, we plot the reduced takeoff velocity  $U/U^*$  as a function of the degree of symmetry  $\varepsilon = r'/r$ , for different ranges of radius  $r$ . We observe that  $U/U^*$  is sensitive both to the size  $r$  of the larger droplet (as discussed in Figure 2a and expressed by Eq. 1), and to the parameter  $\varepsilon$ : the larger the asymmetry (that is, the smaller  $\varepsilon$ ), the slower the takeoff. A change in  $\varepsilon$  by typically 25 % induces a modification of the jumping velocity by a factor 2. Hence, asymmetry impacts the dynamics of jumping much more than adhesion (found in Eq. 1 to decrease  $U$  by only 7 %). For simplicity here, we analyze asymmetry effects by taking  $\alpha = 1$  (negligible adhesion). In addition, if we also neglected viscosity, we would write transfer of momentum  $(m + m')U = m'v'$ , denoting  $v' \approx r'/\tau'$  and  $\tau' \approx 2\sqrt{\rho r'^3/\gamma}$  as the merging velocity and time of the smaller droplet. This yields  $U = U^* \varepsilon^{5/2}/2(1 + \varepsilon^3)$  [32], a prediction drawn with a dashed line in Figure 2b. This behavior is found to capture asymptotically the data at large  $r$  (black symbols). Smaller droplets are

slower, which we understand mostly as a consequence of the viscous dissipation described above. We generalize Eq. 1 to the case of asymmetric merging by rewriting the momentum balance as:  $(m + m')U = m'v' - P'_v - P_v$ , using the same notations as previously. On the one hand, we have  $P'_v \approx F'_v \tau'$ , where the viscous force  $F'_v \approx \eta \Delta v' \Omega'$  is integrated over the merging time  $\tau'$ . On the other hand, we assume  $P_v = P'_v$  because the small drop induces fluid motion in the large one at its own scale, as shown in simulations of merging drops by Eiswirth *et al.* [35]. Hence, we get an analytical expression for the jumping velocity  $U$  in an asymmetric configuration:

$$U \approx U^* \left[ \frac{\varepsilon^{5/2}}{2(1 + \varepsilon^3)} - 2Oh \frac{\varepsilon^2}{1 + \varepsilon^3} \right] \quad (2)$$

Despite the small size of droplets, the Ohnesorge number  $Oh = \eta/(\rho\gamma r)^{1/2}$  remains small ( $< 0.2$ ), so that  $U/U^*$  simply increases with  $\varepsilon$  at fixed  $r$ , and with  $r$  at fixed  $\varepsilon$ , as observed in Figure 2b. As asymmetry vanishes ( $\varepsilon \rightarrow 1$ ), Eq. 2 reduces to Eq. 1 (with  $\alpha = 1$  since we neglected adhesion). Drawn in Figure 2b for three ranges of increasing radii (red, blue and black areas), Eq. 2 is observed to show a fair agreement with the data. More generally, it shows how the conjunction of asymmetry and microscale affects drop departure, a key feature for understanding and tailoring the efficiency of antifogging materials.

## Droplet flight and landing

After takeoff, drops follow quasi-vertical paths (Figure 1c) until falling back to the substrate. We discuss here the flight of microdrops ( $r \leq 17 \mu\text{m}$ ) formed after coalescence. We denote their radius as  $R = (r^3 + r'^3)^{1/3}$  (volume conservation), and we report in Figure 3a the trajectory  $z(t)$  for a drop with radius  $R = 12.9 \pm 0.7 \mu\text{m}$  departing at  $U = 29 \pm 2 \text{ cm/s}$ . The trajectory is observed to be highly asymmetric. While the ascending phase occupies 20 % of the flight time, the descending phase takes much longer, a consequence of the efficient action of air viscosity at microscales. This friction is also responsible for the modest maximum height ( $H = 740 \mu\text{m}$ ) reached by the drop after less than 6 ms. The Reynolds number in air is  $Re = \rho_a U R / \eta_a$ , with  $U$  the jumping velocity,  $\rho_a$  and  $\eta_a$  the air density and viscosity. At microscales,  $Re$  is smaller than unity and Stokes drag  $F = 6\pi\eta_a R \dot{z}$  is the main source of friction [24]. Hence, the successive phases of rise and descent can be expressed by a balance between drag, inertia and gravity which yields the speed  $\dot{z}$  as a function of time  $t$ :

$$\dot{z}(t) = (U + g\tau_a)e^{-t/\tau_a} - g\tau_a \quad (3)$$

where the braking time  $\tau_a$  is equal to  $(2/9)\rho R^2/\eta_a$ . Microdrops trajectories markedly differ from that of drops larger than  $100 \mu\text{m}$ . For these, the drag force becomes negligible and the motion results from an equilibrium between inertia and gravity, which classically results in parabolic motion.

The inset in Figure 3a shows such a symmetric trajectory for a drop with radius  $R = 287 \pm 3 \mu\text{m}$  departing at  $U = 11 \pm 1 \text{ cm/s}$ , together with its parabolic fit drawn in red.

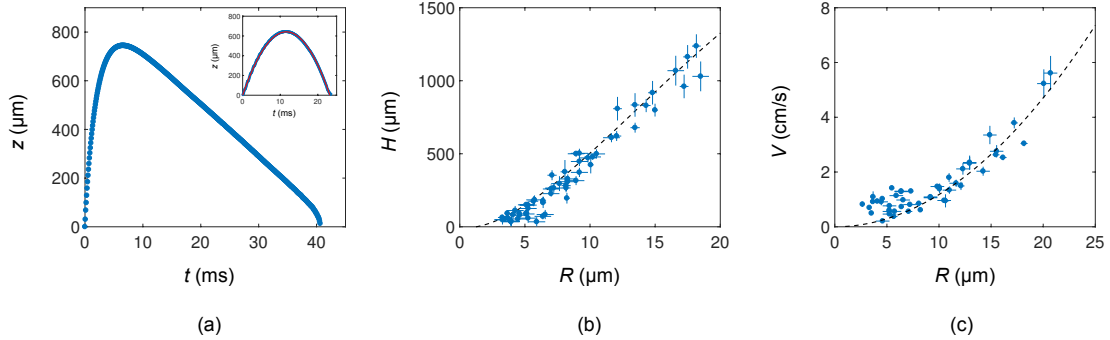


**Figure 3. Flight of departing drops after takeoff.** (a) Trajectory  $z(t)$  of a drop with radius  $R = 12.9 \pm 0.7 \mu\text{m}$  after its ejection. The vertical jumping velocity is  $U = 29 \pm 2 \text{ cm/s}$ . Inset: trajectory  $z(t)$  of a departing drop with radius  $R = 287 \pm 3 \mu\text{m}$ . The trajectory is nicely fitted by a parabola (red solid line) and the vertical jumping velocity is  $U = 11 \pm 2 \text{ cm/s}$ . (b) Maximum measured height  $H$  reached during flight as a function of radius  $R$ . The dashed line represents the theoretical height  $H = U\tau_a - g\tau_a^2 \ln(1 + U/g\tau_a)$ . (c) Absolute terminal velocity  $V$  as a function of radius  $R$ . The dashed line corresponds to the velocity given by the equilibrium between gravity and Stokes drag,  $V = (2/9)\rho g R^2 / \eta_a$ .

From our observations we can also extract a useful, practical quantity that is, the maximum height  $H$  reached by the drop and plotted in Figure 3b [27–29]. Integrating Eq. 3 yields  $z(t) = \tau_a(U + g\tau_a)(1 - e^{-t/\tau_a}) - g\tau_a t$ , whose maximum is:

$$H = U\tau_a - g\tau_a^2 \ln\left(1 + \frac{U}{g\tau_a}\right) \quad (4)$$

The main parameter in the latter equation is the radius  $R$ , both contained in the departing velocity  $U$  (Eq. 1) and in the braking time  $\tau_a$  (Eq. 3). At microscales,  $\tau_a$  is small so that  $H$  increases with  $R$ , as  $R^{3/2}$ . Eq. 4 predicts that  $H(R)$  reaches a maximum around  $R \approx 50 \mu\text{m}$ , a size larger than those studied in this paper. More generally, Eq. 4 drawn with a dashed line in Figure 3b without adjustable parameter nicely describes the data. In the presence of a wind, in the range of 1-10 m/s, the air boundary layer at a centimeter size solid surface expelling dew has a thickness of about  $100 \mu\text{m}$ , showing that most drops can escape this layer and be entrained by the wind - an interesting property if the substrate is horizontal for avoiding the redeposition of dew. For vertical substrate,  $H$  is the typical distance of ejection, after which droplets can fall under the action of gravity. This quantity is also useful to size the so-called phase-change thermal diodes (rectifying heat transfer [36]) by fixing the maximum gap for which jumping drops can be collected by a solid plate above the jumping stage.

On descent, drops quickly reach their terminal velocity  $V$ , plotted in Figure 3c as a function of the radius  $R$  and compared with the prediction  $V = g\tau_a$  (dashed line). The fit is convincing except at small radius ( $R \leq 8 \mu\text{m}$ ) where  $V$  can be as much as ten times larger than predicted. This

discrepancy may originate from a charge effect [37] adding an electrostatic attractive contribution to the force balance, which is dominant at small substrate distances (*i.e.* at small  $R$ ). This supplementary attraction is found to become significant at a distance of about  $200\ \mu\text{m}$ , which corresponds (in Figure 3b) to a radius of about  $7.5\ \mu\text{m}$ , the size below which the gravitational prediction does not apply.

Droplets finally return to the substrate, which they impact at the velocity  $V$ . We study the landing for both condensed drops ( $2.7\ \mu\text{m} \leq R \leq 22.7\ \mu\text{m}$  and  $2\ \text{cm/s} \leq V \leq 15\ \text{cm/s}$ ) and water sprayed onto the surface ( $25\ \mu\text{m} \leq R \leq 160\ \mu\text{m}$  and  $2\ \text{cm/s} \leq V \leq 100\ \text{cm/s}$ ), and report in Figure 4 the behaviour of drops after impact: either they bounce (green data), as expected on a repellent material, or they stick (red data split between sprayed (squares) and condensed droplets (empty circles)). Only drops with large size ( $R$ ) and velocity ( $V$ ) are observed to bounce. Conversely, none of the droplets formed by condensation get reflected by the material from which they were ejected. Hence, dew repellency is found to be more demanding than dew ejection, which we now discuss.

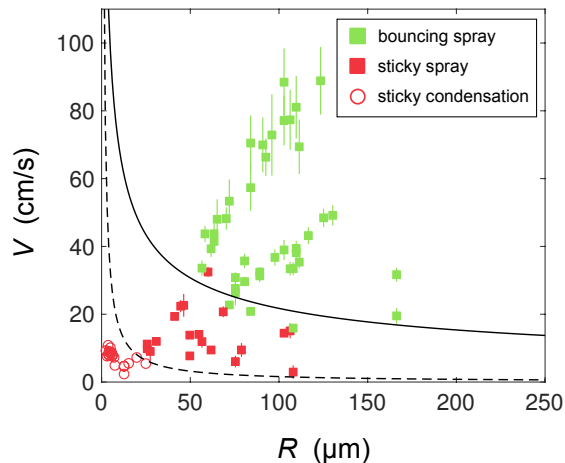


**Figure 4. Phase diagram of droplets behaviour at landing.** The drop radius and velocity are denoted as  $R$  and  $V$ . Green color indicates bouncing and red color indicates sticking. Dots and squares mean that drops are made from condensation or from a spray, respectively. The solid line expresses the balance between adhesion and inertia (Eq. 5). The dashed line represents the threshold of bouncing dictated by viscosity,  $V^* \approx \eta/\rho R$ .

Our experiments probe the very unusual situation of microdrops impacting a solid at a small velocity (red circles). The corresponding Reynolds number  $Re = \rho R V / \eta$  is of order unity or even smaller. Hence, even in the limit of a strictly non-adhesive material ( $\theta_r = 180^\circ$ ), drops should stick when the viscous dissipation at impact exceeds the kinetic energy.  $Re = 1$  provides the threshold  $V^* = \eta/\rho R$  above which we leave this regime. This frontier is marked with a dashed line in Figure 4 and it is found to enclose all the data for dew. Being above this dashed line does not guarantee bouncing either. The Weber number  $We = \rho V^2 R / \gamma$  controlling liquid deformation at impact in

this domain remains modest, on the order of 0.1. Hence, for the sake of simplicity we consider that impacting water contacts the substrate with a radius of order  $R$ , with a contact line dissipation of order  $\pi R^2 \gamma (1 + \cos \theta_r)$ . Drops will stick if this quantity exceeds the kinetic energy at impact  $2\pi R^3 \rho V^2 / 3$ . The balance between these two energies yields a minimum velocity  $V^*$  required for repellency:

$$V^* \approx \sqrt{\frac{3\gamma}{2\rho R} (1 + \cos \theta_r)} \quad (5)$$

Drawn with a solid line in Figure 4, Eq. 5 nicely captures the frontier between bouncing and sticking. More generally, if we model the behaviour of droplets after ejection using Eq. 3, we find  $g\tau_a > V^*$  as a criterion for bouncing. Both the dependencies of  $\tau_a$  and  $V^*$  with  $R$  being known, we deduce a minimum radius  $R^* = [243 \eta_a^2 \gamma (1 + \cos \theta_r) / 8\rho^3 g^2]^{1/5}$ , for bouncing to be around 60  $\mu\text{m}$ . Such drops are larger than that obtained after condensation which confirms the inability of condensed drops to bounce. It may seem surprising that an antifogging surface is unable to reflect the water ejected from it, but this is just a consequence of their slowness at impact. The only possibility for such a drop to bounce is to meet another one at impact [38, 39].

In summary, we have provided quantitative measurements of the jumping velocity of coalescing droplets with radii ranging from 1  $\mu\text{m}$  to 1 mm. Experiments at small scales were made possible by the use of highly non-adhesive materials, which enables water to remain mobile even at microscales. We report that the jumping velocity obeys the classical inertio-capillary scaling down to 5  $\mu\text{m}$ , below which strong deviations are observed and interpreted as a consequence of viscous dissipation. The asymmetry of merging is shown to be another cause of reduced jumping efficiency. We characterized the flight, maximum height, descent kinetics and landing of jumping microdroplets. Air viscosity rapidly stops ejected drops that later fall so slowly that they cannot bounce after impact. Our findings might help to design new antifogging properties where condensation produces drops large enough to be efficiently evacuated from the surface. The coupling of this motion with a lateral wind would be interesting to study, as well as the case where drops take off with solid particles (contamination or ballistospore) [40–43]. Another natural development of this study would be to understand how more than two drops merging on the surface are ejected.

## Acknowledgements

We thank Julien Husson and Alexandra Zak for the fabrication of the glass micro-needles. Research carried at Brookhaven National Laboratory is supported by the U.S. Department of Energy, Office of Basic Energy Sciences, under Contract No. DE-SC0012704 and used resources of the Center for Functional Nanomaterials, which is a U.S. DOE Office of Science Facility. P.L. thanks the Ecole

polytechnique for the financial support (Monge Fellowship). T.M. thanks the Direction Générale de l'Armement (DGA) for contributing to the financial support, Rose-Marie Sauvage and Thierry Midavaine for their constant interest, and Thalès for cofunding this project. We finally thank Romain Labbé for help in the design of the experiments.

## References

- [1] D. L. Hu, B. Chan, and J. W. M. Bush, "The hydrodynamics of water strider locomotion," *Nature*, vol. 424, pp. 663–666, 2003.
- [2] X. Gao and L. Jiang, "Biophysics: water-repellent legs of water striders," *Nature*, vol. 432, pp. 36–36, 2004.
- [3] J. W. M. Bush and D. L. Hu, "Walking on water: biolocomotion at the interface," *Annu. Rev. Fluid Mech.*, vol. 38, pp. 339–369, 2006.
- [4] R. Blossey, "Self-cleaning surfaces—virtual realities," *Nature Materials*, vol. 2, pp. 301–306, 2003.
- [5] J. C. Bird, R. Dhiman, H.-M. Kwon, and K. K. Varanasi, "Reducing the contact time of a bouncing drop," *Nature*, vol. 503, pp. 385–388, 2013.
- [6] Y. Liu, L. Moevius, X. Xu, T. Qian, J. M. Yeomans, and Z. Wang, "Pancake bouncing on superhydrophobic surfaces," *Nature Physics*, vol. 10, pp. 515–519, 2014.
- [7] C. Shi, X. Cui, X. Zhang, P. Tchoukov, Q. Liu, N. Encinas, M. Paven, F. Geyer, D. Vollmer, Z. Xu, H.-J. Butt, and H. Zeng, "Interaction between air bubbles and superhydrophobic surfaces in aqueous solutions," *Langmuir*, vol. 31, pp. 7317–7327, 2015.
- [8] W. A. Calder, "Temperature relations and underwater endurance of the smallest homeothermic diver, the water shrew," *Comparative Biochemistry and Physiology*, vol. 30, pp. 1075–1082, 1969.
- [9] M. R. Flynn and J. W. M. Bush, "Underwater breathing: the mechanics of plastron respiration," *Journal of Fluid Mechanics*, vol. 608, pp. 275–296, 2008.
- [10] A. Balmert, H. F. Bohn, P. Ditsche-Kuru, and W. Barthlott, "Dry under water: Comparative morphology and functional aspects of air-retaining insect surfaces," *Journal of Morphology*, vol. 272, pp. 442–451, 2011.
- [11] C. Cottin-Bizonne, J.-L. Barrat, L. Bocquet, and E. Charlaix, "Low-friction flows of liquid at nanopatterned interfaces," *Nature Materials*, vol. 2, pp. 237–240, 2003.
- [12] J. Ou, B. Perot, and J. P. Rothstein, "Laminar drag reduction in microchannels using ultra-hydrophobic surfaces," *Physics of Fluids*, vol. 16, pp. 4635–4643, 2004.
- [13] A. Tuteja, W. Choi, M. Ma, J. M. Mabry, S. A. Mazzella, G. C. Rutledge, G. H. McKinley, and R. E. Cohen, "Designing superoleophobic surfaces," *Science*, vol. 318, pp. 1618–1622, 2007.
- [14] A. Steele, I. Bayer, and E. Loth, "Inherently superoleophobic nanocomposite coatings by spray atomization," *Nano letters*, vol. 9, pp. 501–505, 2008.
- [15] J. B. Boreyko and C.-H. Chen, "Self-propelled dropwise condensate on superhydrophobic surfaces," *Physical Review Letters*, vol. 103, p. 184501, 2009.
- [16] K. M. Wisdom, J. A. Watson, X. Qu, F. Liu, G. S. Watson, and C.-H. Chen, "Self-cleaning of superhydrophobic surfaces by self-propelled jumping condensate," *Proceedings of the National Academy of Sciences*, vol. 110, pp. 7992–7997, 2013.
- [17] C. Lv, P. Hao, Z. Yao, Y. Song, X. Zhang, and F. He, "Condensation and jumping relay of droplets on lotus leaf," *Applied Physics Letters*, vol. 103, p. 021601, 2013.

- [18] F. Liu, G. Ghigliotti, J. J. Feng, and C.-H. Chen, “Numerical simulations of self-propelled jumping upon drop coalescence on non-wetting surfaces,” *Journal of Fluid Mechanics*, vol. 752, pp. 39–65, 2014.
- [19] F.-C. Wang, F. Yang, and Y.-P. Zhao, “Size effect on the coalescence-induced self-propelled droplet,” *Applied Physics Letters*, vol. 98, p. 053112, 2011.
- [20] R. Enright, N. Miljkovic, J. Sprittles, K. Nolan, R. Mitchell, and E. N. Wang, “How coalescing droplets jump,” *ACS Nano*, vol. 8, pp. 10352–10362, 2014.
- [21] M.-K. Kim, H. Cha, P. Birbarah, S. Chavan, C. Zhong, Y. Xu, and N. Miljkovic, “Enhanced jumping-droplet departure,” *Langmuir*, vol. 31, pp. 13452–13466, 2015.
- [22] T. Mousterde, G. Lehoucq, S. Xavier, A. Checco, C. T. Black, A. Rahman, T. Midavaine, C. Clanet, and D. Quéré, “Antifogging abilities of model nanotextures,” *Nature Materials*, vol. 16, pp. 658–663, 2017.
- [23] M. D. Mulroe, B. R. Srijanto, S. F. Ahmadi, C. P. Collier, and J. B. Boreyko, “Tuning superhydrophobic nanostructures to enhance jumping-droplet condensation,” *ACS Nano*, vol. 11, no. 8, pp. 8499–8510, 2017.
- [24] F. Liu, G. Ghigliotti, J. J. Feng, and C.-H. Chen, “Self-propelled jumping upon drop coalescence on leidenfrost surfaces,” *Journal of Fluid Mechanics*, vol. 752, pp. 22–38, 2014.
- [25] Z. Liang and P. Keblinski, “Coalescence-induced jumping of nanoscale droplets on superhydrophobic surfaces,” *Applied Physics Letters*, vol. 107, p. 143105, 2015.
- [26] H. Cha, C. Xu, J. Sotelo, J. M. Chun, Y. Yokoyama, R. Enright, and N. Miljkovic, “Coalescence-induced nanodroplet jumping,” *Physical Review Fluids*, vol. 1, p. 064102, 2016.
- [27] B. Peng, S. Wang, Z. Lan, W. Xu, R. Wen, and X. Ma, “Analysis of droplet jumping phenomenon with lattice boltzmann simulation of droplet coalescence,” *Applied Physics Letters*, vol. 102, p. 151601, 2013.
- [28] G. S. Watson, M. Gellender, and J. A. Watson, “Self-propulsion of dew drops on lotus leaves: a potential mechanism for self cleaning,” *Biofouling*, vol. 30, pp. 427–434, 2014.
- [29] G. S. Watson, L. Schwarzkopf, B. W. Cribb, S. Myhra, M. Gellender, and J. A. Watson, “Removal mechanisms of dew via self-propulsion off the gecko skin,” *Journal of the Royal Society Interface*, vol. 12, p. 20141396, 2015.
- [30] J. Liu, H. Guo, B. Zhang, S. Qiao, M. Shao, X. Zhang, X.-Q. Feng, Q. Li, Y. Song, L. Jiang, and J. Wang, “Guided self-propelled leaping of droplets on a micro-anisotropic superhydrophobic surface,” *Angewandte Chemie*, vol. 128, pp. 4337–4341, 2016.
- [31] A. Checco, A. Rahman, and C. T. Black, “Robust superhydrophobicity in large-area nanostructured surfaces defined by block-copolymer self assembly,” *Advanced Materials*, vol. 26, pp. 886–891, 2014.
- [32] T. Mousterde, T.-V. Nguyen, H. Takahashi, C. Clanet, I. Shimoyama, and D. Quéré, “How merging droplets jump off a superhydrophobic surface: measurements and model,” *Physical Review Fluids*, vol. 2, p. 11200, 2017.
- [33] B. Zhang, X. Chen, J. Dobnikar, Z. Wang, and X. Zhang, “Spontaneous wenzel to cassie dewetting transition on structured surfaces,” *Physical Review Fluids*, vol. 1, p. 073904, 2016.
- [34] H. Vahabi, W. Wang, S. Davies, J. M. Mabry, and A. K. Kota, “Coalescence-induced self-propulsion of droplets on superomniphobic surfaces,” *ACS applied materials & interfaces*, vol. 9, no. 34, pp. 29328–29336, 2017.
- [35] R. Eiswirth, H.-J. Bart, A. Ganguli, and E. Kenig, “Experimental and numerical investigation of binary coalescence: Liquid bridge building and internal flow fields,” *Physics of Fluids*, vol. 24, p. 062108, 2012.
- [36] J. B. Boreyko, Y. Zhao, and C.-H. Chen, “Planar jumping-drop thermal diodes,” *Applied Physics Letters*, vol. 99, no. 23, p. 234105, 2011.

- [37] N. Miljkovic, D. J. Preston, R. Enright, and E. N. Wang, “Electrostatic charging of jumping droplets,” *Nature communications*, vol. 4, p. 2517, 2013.
- [38] C. Lv, P. Hao, Z. Yao, and F. Niu, “Departure of condensation droplets on superhydrophobic surfaces,” *Langmuir*, vol. 31, pp. 2414–2420, 2015.
- [39] X. Chen, R. S. Patel, J. A. Weibel, and S. V. Garimella, “Coalescence-induced jumping of multiple condensate droplets on hierarchical superhydrophobic surfaces,” *Scientific Reports*, vol. 6, p. 18649, 2016.
- [40] J. Turner and J. Webster, “Mass and momentum transfer on the small scale: How do mushrooms shed their spores?,” *Chemical Engineering Science*, vol. 46, pp. 1145–1149, 1991.
- [41] A. Pringle, S. N. Patek, M. Fischer, J. Stolze, and N. P. Money, “The captured launch of a ballistospore,” *Mycologia*, vol. 97, pp. 866–871, 2005.
- [42] X. Noblin, S. Yang, and J. Dumais, “Surface tension propulsion of fungal spores,” *Journal of Experimental Biology*, vol. 212, pp. 2835–2843, 2009.
- [43] F. Liu, R. L. Chavez, S. Patek, A. Pringle, J. J. Feng, and C.-H. Chen, “Asymmetric drop coalescence launches fungal ballistospores with directionality,” *Journal of The Royal Society Interface*, vol. 14, p. 20170083, 2017.